Attosecond Coherent Control of Single and Double Photoionization in Argon

C. W. Hogle, X. M. Tong, L. Martin, M. M. Murnane, H. C. Kapteyn, and P. Ranitovic

Phys. Rev. Lett. **115**, 173004 — Published 22 October 2015

DOI: 10.1103/PhysRevLett.115.173004

Attosecond Coherent Control of Single and Double Photoionization in Argon

C. W. Hogle[1], X. M. Tong[2], L. Martin[1], M. M. Murnane[1], H. C. Kapteyn[1], P. Ranitovic[1,3,4]

[1]*JILA and Department of Physics, University of Colorado and NIST, Boulder, CO 80309, USA*

[2]*Division of Materials Science, Faculty of Pure and Applied Science, University of Tsukuba, Ibaraki 305-8573, Japan*

[3]*Lawrence Berkeley National Lab, 1 Cyclotron Road, Berkeley CA, 94720*

[4]*ELI-ALPS, ELI-Hu Nkft, Dugonics ter 13, Szeged H6720, Hungary.*

Abstract

Ultrafast high harmonic beams provide new opportunities for coherently controlling excitation and ionization processes in atoms, molecules and materials on attosecond time scales by employing multiphoton two-pathway electron-wave packet quantum interferences. Here we use spectrally tailored and frequency tuned vacuum and extreme ultraviolet harmonic combs, together with two phase-locked infrared laser fields, to show how the total single *and* double photoionization yields of argon can be coherently modulated by controlling the relative phases of both optical and electronic-wave packet quantum interferences. This work is the first to apply quantum control techniques to double photoionization, which is a fundamental process where a single, high-energy photon ionizes two electrons simultaneously from an atom.

In the pioneering coherent quantum control experiments, two-pathway interference processes were theoretically predicted and experimentally demonstrated in the 1980s and 1990s using visible and infrared (IR) laser pulses [1-5]. However, due to the low intensity and long duration of the laser pulses available for those early experiments, the systems that could be studied were limited to low ionization potential species [5,6]. To extend coherent control concepts to higher photon energies and shorter time scales, and access core-hole, inner-valance or doubly-excited systems where autoionization, Auger decay, interatomic Coulomb decay, and other ultrafast processes play a role, ultrafast pulses at high photon energies are required. Table-top high harmonics represent a unique light source that is perfectly synchronized to the driving laser, which can be used to manipulate the fastest electron and molecular dynamics in matter [7-15]. Very recently it was realized that a series of vacuum ultraviolet (VUV) and extreme ultraviolet (XUV) high-harmonics can be used as a tool for exciting and controlling electron and nuclear wave-packet dynamics on attosecond time scales [16-23]. For example, multicolor XUV and IR beams can create so-called dark pulses [24] in a resonant multiphoton ionization of He, by controlling both the amplitude and the frequency of the XUV harmonics [18].

In this work we show that by spectrally separating a comb of high harmonics into VUV and XUV components, we can coherently populate Rydberg states of Ar and Ar^+, close to the single and double ionization thresholds. Then, in the presence of two IR fields, one co-propagating and phase-locked with the VUV/XUV pump pulse and another that is time-delayed relative to the combined VUV/XUV/IR pump pulse, we show that we can coherently control both Ar^+ and Ar^{++} total yields using two-quantum-pathway electron wave packet interference processes. Furthermore, by tuning the energy of the VUV/XUV photons around different resonant Ar^* and Ar^{+*} states, we demonstrate an ability to fine-tune the phases of the optical and

quantum interferences produced by the combined action of the IR laser and VUV/XUV harmonic fields. This work demonstrates that attosecond coherent control methods can manipulate double ionization processes on attosecond time scales, where electron-electron interactions play an important role. Double photoionization is a fundamental mechanism where a single photon can ionize two electrons simultaneously from an atom, providing insight into electron/electron dynamical correlation processes [25-28]. Understanding and coherently controlling these correlations in simple atoms and molecules, where theoretical models are possible, will help develop the more advanced concepts necessary to control ultrafast dynamics in complex molecular systems [29] or novel, strongly-correlated materials [30].

In our experiment, we used a high-power (25 W), high repetition rate (10 kHz) Ti:sapphire laser system coupled to a COLTRIMS setup. Most of the laser energy (≈1.7 mJ) was coupled into a waveguide filled with Ar to generate harmonics, which were refocused into a supersonic Ar gas target using a pair of XUV multilayer mirrors, which have a reflectance as shown in Fig. 1. The central photon energies of the harmonics were controlled by tuning the gas pressure in the waveguide [18]. COLTRIMS enables simultaneous detection of ion and electron 3D momenta [7,31,32], allowing us to analyze both single and double ionization events in coincidence with electrons. The rest of the laser energy (≈0.8 mJ) was sent though a delay stage, and spatially and temporally recombined with the high harmonic beam in a collinear geometry using a mirror with a whole. We also co-propagate a small amount of the IR driving laser field with the HHG beam, which serves as a reference beam that interferes with the time-delayed IR probe pulse. The duration of the HHG pulse was ≈10 fs, while the IR pulse duration was 30 fs. The intensity of the co-propagating IR pulse was $3x10^{11}$ W/cm^2, while the time-delayed probe IR intensity was $3x10^{12}$ W/cm^2, and wavelength was 784 nm. For the theoretical parameters, we used cosine IR

pulses at zero delay, and the attosecond pulses trains were locked to the maximum of the pump IR pulse. The pump VUV/XUV/IR pulse was fixed at zero delayed, and the probe IR pulse was delayed.

Spectral selection of the VUV (7ω, 9ω, and 11ω) and XUV (25ω, 27ω) components was achieved by a multilayer mirror optimized for 42 eV, which also reflects some of the laser light at a frequency ω. The schematic of the experimental setup and the relevant Ar energy levels, as well as the HHG photon energies and amplitudes, are shown in Fig. 1. By tuning the pressure of the harmonic-generation medium, we can blue-shift the central energy of each harmonic order so that the VUV harmonics (7ω and 9ω) are either mostly non-resonant (red in Fig. 1) or mostly resonant (blue) with Ar^* Rydberg states. Moreover, because of the narrow bandwidth of the multilayer mirrors coated to reflect photon energies around 42 eV, this pressure tuning results in either one dominant (25ω) or two dominant XUV (25ω and 27ω) harmonics that can directly double ionize and excite Ar^+ just below the double ionization threshold. By introducing time-delayed probe IR field, we can couple the states excited by the VUV/XUV HHG directly into the single/double ionization continuum, while also controlling the phases of the interfering electron wave-packets. This results in a modulation of the total Ar^+ and Ar^{++} yields. As shown in Fig. 1, the Ar ground state can be coupled to both the Ar^+ and the Ar^{++} continua via two different electron-wavepacket interfering pathways for each final state, with the resultant continuum electron energies equivalent to 10ω and 27ω respectively. Specifically, the dominant interfering pathways are $9\omega + \omega$ and $11\omega - \omega$, and $25\omega + 2\omega$ and 27ω, in the VUV and XUV regions, respectively.

To distinguish the optical from quantum interference effects, in Fig. 1 (inset a) we plot the calculated Ar^+ yield modulation for resonant and nonresonant VUV fields, when only one IR

probe field is present, where it acts as a control pulse that ionizes the Ar^* states. Two striking features are obvious as the probe IR pulse is delayed relative to the VUV pulse: first, the amplitude of the oscillation in the resonant case is significantly smaller compared with the nonresonant case; and second, the yields oscillate out of phase. Since in this case only one IR field is present, *only* quantum wave packet interferences can play a role in the modulation of the total Ar^+ yield, i.e. interfering pathways $9\omega + \omega$ and $11\omega - \omega$. In this case the quantum phase depends on the exact energy of the VUV harmonics and their positions relative to the Ar^* Floquet states dressed by the IR field [33,34]. The amplitude of the oscillation changes due to the different excitation probability as the 9^{th} harmonic is tuned in and out of the Ar^* resonances. By adding a second, weak IR pulse, that we lock to the VUV pulse, we start mixing optical and quantum interferences as the IR probe pulse is delayed with respect to the VUV/IR pump pulses [17,19]. The first striking feature we see in Fig. 1 (inset b) is that the addition of the reference IR pulse does not significantly change the amplitude and the phase of the Ar^+ yield oscillation in the nonresonant case, which is counterintuitive considering the fact the optical interference of the two IR pulses, and the resultant intensity modulation should drive the periodicity of the total yield oscillation. This, however, changes as we slightly shift the central energy of the VUV harmonics to make them resonant with the IR-dressed Ar^* states. As we see in the resonant case, the total yield oscillation is dominated by a full-optical-cycle periodicity. We note that for the simplicity of the presentation, we use a resonant and nonresonat vocabulary even though in the non-resonant case the 9^{th} harmonic is partially resonant with the unperturbed 3d state or partially seen in the SI continuum when the harmonics were blue-shifted. While in the presence of the IR field the resonances are shifted, broadened and dressed [18], we show only the relevant unperturbed resonances for the simplicity of the presentation.

We can also coherently populate Ar^{**}, Ar^{+*} and Ar^{++} states, by using higher-energy XUV harmonics. Here, by adding a time-delayed IR probe field, the ground state of Ar can be projected to the Ar^{++} continuum either directly by the 27ω harmonic, or by a resonant three-photon absorption ($25\omega + 2\omega$). Similar to the case of Ar^{+}, these two-pathway quantum interferences mean that the total Ar^{++} yield is also modulated. We note that in this double-ionization case, some of the autoionizing Ar^{**} states decay on femtosecond time-scales [35], which means that the amplitude of the three-photon absorption pathway decreases during the interference process. Quantifying this time-dependent contribution to the amplitude of one of the interfering electron wave packets requires advanced calculations that take into account the influence of the laser field on the creation of the doubly excited states in argon, which is beyond our theoretical capabilities at moment. We note that all the theoretical studies were performed by solving the time-dependent Schrödinger equation in a single active electron approximation using a model potential [36]. The detailed numerical methods used in our simulations can be found in Ref. [37].

Figure 2 shows the experimental and theoretical Ar^{+} yields as a function of time-delay between the pump and probe pulses, while the insets zoom-in around time-zero to show the modulation of the total yields on attosecond time-scales. For the experimental data shown in Fig. 2, we used two IR pulses: pump IR pulse was copropagated and locked in phase with the VUV harmonics, and the probe IR pulse was time delayed. Figure 2(a) shows the Ar^{+} yield when the harmonics were mostly not resonant with Ar^{*} states, so the Ar^{+} yield enhancement only occurs when the VUV+IR pump and IR probe pulses overlap. We note that the small yield enhancement for the long IR delays tells us the VUV/IR pump pulse was partially exciting Ar^{*} states. The scan around time zero shows that the yield is modulated with half-an-optical cycle periodicity. The

theoretical data shown in Figs. 1(inset b) and 2(b) are in a good agreement with the data. Note that the theoretical data shown in Fig. 2(b) reveal that the periodicity is not exactly half-an-optical cycle (i.e. 1.3 fs), and can rather be seen as two different full-cycle (ω) oscillations almost, but not perfectly dephased (i.e. 1.2 fs and 1.4 fs spacing between maxima). The mixing of optical and quantum interferences using one color IR pump/probe experiments was first reported by Blanchet *et al*. in Cs [4,5]. Here we show how additional frequency tuning of the VUV beam can control the relative phases of the optical and quantum interferences in systems with higher ionization potential. Figure 2(c) shows a striking difference in the Ar^+ yield modulation as we slightly tune the central frequency of the VUV pulse into Ar^* resonances. The step-function shape of the femtosecond Ar^+ yield confirms that 7ω and 9ω were mostly resonant with Ar Rydberg states, while the attosecond scan shows that a simple change of the VUV central energy changes the Ar^+ yield periodicity from half- to full-cycle oscillations. The theory in Fig. 2(d) reproduces the experimental results. We believe that the main reason for the switch of the yield periodicities lays in the fact that quantum phase flips (see Fig. 1 upper inset) as we scan the VUV harmonic energies across the IR-dressed Ar^* resonances, while the phase of the optical interferences stays the same [34].

To resolve the total Ar^+ yield modulation in the frequency domain, we measured photoelectron energies in coincidence with the Ar^+ ions. In Fig. 3 we show that the modulation of the total Ar^+ yield arises mainly from the interferences in the 10ω photoelectron band. Note that in the non-resonant case, the effective 10^{th} harmonic band ($9\omega + \omega$) sits just above the ionization threshold (Fig. 3a), while in the resonant case, part of the 9^{th} harmonic appears above the ionization potential. In this case, each of the photoelectron bands, labeled as 9ω, 10ω and 11ω in Fig. 3(c), oscillates with full optical cycle periodicity but with different phases, as indicated by the arrows,

introducing small modulations in the total Ar^+/e^- yield. See the supplementary material for more detail on how small changes in the VUV central energy change the phases of the photoelectron bands and total Ar^+ yield enhancement and modulation in the resonant case.

Figure 4 shows, experimentally and theoretically, that the attosecond coherent quantum control can be extended to a double photoionization process. As we blue-shift the XUV harmonics the multilayer mirrors reflect either two harmonics of similar amplitudes (25ω and 27ω) for the non-blueshifted case, or a single dominant XUV harmonic for the blueshifted case. Figure 4(a) shows the experimental Ar^{++} yield modulation as a function of IR delay on attosecond timescales, when two dominant XUV harmonics are present. Under these conditions, there are two coherent quantum pathways projecting the Ar ground state into the double ionization continuum (i.e. 27ω and 25ω + 2ω), which results in a half-optical cycle oscillation of the total Ar^{++} yield, even though the two IR pulses introduce intensity modulation due to the optical interferences. Figure 4(c) shows the double ionization yield as a function of delay when the harmonics were blueshifted, so that only one harmonic is strongly reflected. In this case, the Ar^{++} yield modulates with full optical-cycle periodicity. In our current model, we cannot simulate single-photon double ionization of Ar directly due to the complexity of the electron-electron interactions in the intense IR fields. Simulating the Ar^{+*} and Ar^{**} excitations in the presence of the IR field is particularly challenging. However, we know that Ar double ionization can come from (a) shake-off or IR-ionization of states excited by the XUV photoionization (including double-excitation), and (b) laser enabled Auger decay of sub-valence states [35,38]. Both of these processes require that the total energy of $Ar^+ + e^-$ is above the double ionization threshold. Therefore, we calculate the photoelectron energies using the single active electron approximation and integrate the yields above the Ar double ionization threshold. See the SM for more detail on the calculations and the

electrons take in coincidence with Ar^{++} ions. The theoretical results shown in Figs. 4 (b) and (d) nicely reproduce the data, showing half optical cycle oscillations for the non-blueshifted case in (b), and a full optical cycle oscillation in (d). Interestingly, the theoretical double-ion yield plotted as a dashed line in Fig. 4 (d) shows that introduction of a small amount of the 23^{rd} harmonic (see Fig. 1) can be used as a tool for fine control over quantum amplitudes and phases, resulting in fine modulation of the main Ar^{++} full-cycle yield oscillation. These calculations qualitatively reproduce the data and show that the two-pathway electron-wave packet interferences are the main mechanism behind the modulation of the Ar^{++} yield. To quantitatively reproduce the data, though, new theoretical methods have to be developed that would include electron-electron interactions responsible for excitation of the Ar^{+*} and Ar^{**} autoionizing states by the XUV/IR radiation.

In summary, we demonstrate attosecond coherent control of both single and double ionization yields in Ar by frequency tuning and amplitude shaping of VUV and XUV high harmonics, in the presence of IR fields. The three-pulse, multicolor approach demonstrated here extends the attosecond coherent control processes to the double ionization domain, opening the door for using table-top harmonic beams as a novel tool to coherently control electron dynamics in highly excited states where electron-electron interactions play an important role. Also, we showed that below-the-threshold VUV harmonics (i.e. 7^{th} and 9^{th}) generated in Ar HHG medium, can also be used as an attosecond coherent control tool similar to the above-the-threshold attosecond XUV pulse trains. This opens door for using the attosecond VUV harmonics to coherently control the excitation of neutral molecules, and strongly correlated materials.

The authors gratefully acknowledge support from the Army Research Office. XMT was supported by a Grand-in-Aid for Scientific Research (C24540421) from the Japan Society for the Promotion of Science.

References

[1] S. Park, S. Lu, and R. Gordon, J Chem Phys **94**, 8622 (1991).
[2] L. Zhu, V. Kleiman, X. Li, S. P. Lu, K. Trentelman, and R. J. Gordon, Science 77 (1995).
[3] D. Meshulach and Y. Silberberg, Nature **396**, 239 (1998).
[4] V. Blanchet, M. A. Bouchene, O. Cabrol, and B. Girard, Chem Phys Lett **233**, 491 (1995).
[5] V. Blanchet, C. Nicole, M. Bouchene, and B. Girard, Phys Rev Lett **78**, 2716 (1997).
[6] D. Schumacher, B. Lyons, and T. Gallagher, Phys Rev Lett **78**, 4359 (1997).
[7] A. Rundquist, C. Durfee, Z. Chang, C. Herne, S. Backus, M. Murnane, and H. Kapteyn, Science **280**, 1412 (1998).
[8] M. Drescher, M. Hentschel, R. Kienberger, M. Uiberacker, V. Yakovlev, A. Scrinzi, T. Westerwalbesloh, U. Kleineberg, U. Heinzmann, and F. Krausz, Nature **419**, 803 (2002).
[9] E. Turgut, C. La-O-Vorakiat, J. M. Shaw, P. Grychtol, H. T. Nembach, D. Rudolf, R. Adam, M. Aeschlimann, C. M. Schneider, T. J. Silva, M. M. Murnane, H. C. Kapteyn, and S. Mathias, Phys Rev Lett **110**, 197201 (2013).
[10] E. Goulielmakis, M. Uiberacker, R. Kienberger, A. Baltuska, V. Yakovlev, A. Scrinzi, T. Westerwalbesloh, U. Kleineberg, U. Heinzmann, M. Drescher, and F. Krausz, Science **305**, 1267 (2004).
[11] T. Remetter, P. Johnsson, J. Mauritsson, K. Varj Uacute, Y. Ni, F. L Eacute Pine, E. Gustafsson, M. Kling, J. Khan, R. L Oacute Pez-Martens, K. J. Schafer, M. J. J. Vrakking, and A. L Rsquo Huillier, Nat Phys **2**, 323 (2006).
[12] E. Gagnon, P. Ranitovic, X.-M. Tong, C. L. Cocke, M. M. Murnane, H. C. Kapteyn, and A. S. Sandhu, Science **317**, 1374 (2007).
[13] A. S. Sandhu, E. Gagnon, R. Santra, V. Sharma, W. Li, P. Ho, P. Ranitovic, C. L. Cocke, M. M. Murnane, and H. C. Kapteyn, Science **322**, 1081 (2008).
[14] G. Sansone, F. Kelkensberg, J. F. Perez-Torres, F. Morales, M. F. Kling, W. Siu, O. Ghafur, P. Johnsson, M. Swoboda, E. Benedetti, F. Ferrari, F. Lepine, J. L. Sanz-Vicario, S. Zherebtsov, I. Znakovskaya, A. L'Huillier, M. Y. Ivanov, M. Nisoli, F. Martin, and M. J. J. Vrakking, Nature **465**, 763 (2010).
[15] T. Popmintchev, M. C. Chen, D. Popmintchev, and P. Arpin, Science (2012).
[16] P. Johnsson, J. Mauritsson, T. Remetter, A. L'Huillier, and K. J. Schafer, Phys Rev Lett **99**, 233001 (2007).
[17] P. Ranitovic, X. M. Tong, B. Gramkow, S. De, B. DePaola, K. P. Singh, W. Cao, M. Magrakvelidze, D. Ray, I. Bocharova, H. Mashiko, A. Sandhu, E. Gagnon, M. M. Murnane, H. C. Kapteyn, I. Litvinyuk, and C. L. Cocke, New J Phys **12**, 013008 (2010).
[18] P. Ranitovic, X. M. Tong, C. W. Hogle, X. Zhou, Y. Liu, N. Toshima, M. M. Murnane, and H. C. Kapteyn, Phys Rev Lett **106**, 193008 (2011).
[19] N. Shivaram, H. Timmers, X.-M. Tong, and A. Sandhu, Phys Rev Lett **108**, 193002 (2012).
[20] P. Ranitovic, C. W. Hogle, P. Rivière, A. Palacios, X.-M. Tong, N. Toshima, A. González-Castrillo, L. Martin, F. Martín, M. M. Murnane, and H. C Kapteyn, Proceedings of the National Academy of Sciences **111**, 912 (2014).
[21] H. Wang, M. Chini, S. Chen, C.-H. Zhang, F. He, Y. Cheng, Y. Wu, U. Thumm, and Z. Chang, Phys Rev Lett **105**, 143002 (2010).
[22] P. Tzallas, E. Skantzakis, L. Nikolopoulos, G. D. Tsakiris, and D. Charalambidis, Nat Phys **7**, 781 (2011).
[23] E. P. Mansson, D. Guenot, C. L. Arnold, D. Kroon, S. Kasper, J. M. Dahlstrom, E. Lindroth, A. S. Kheifets, A. L'Huillier, S. L. Sorensen, and M. Gisselbrecht, Nat Phys **10**, 207 (2014).
[24] A. Gandman, L. Rybak, and Z. Amitay, Phys Rev Lett (2014).
[25] T. Weber, A. O. Czasch, O. Jagutzki, A. K. Mueller, V. Mergel, A. Kheifets, E. Rotenberg, G. Meigs, M. H. Prior, S. Daveau, A. Landers, C. L. Cocke, T. Osipov, R. Diez Muino, H. Schmidt-Boecking, and R. Doerner, Nature **443**, 1014 (2006).

[26] D. Akoury, K. Kreidi, T. Jahnke, T. Weber, A. Staudte, M. Schoeffler, N. Neumann, J. Titze, L. P. H. Schmidt, A. Czasch, O. Jagutzki, R. A. C. Fraga, R. E. Grisenti, R. Diez Muino, N. A. Cherepkov, S. K. Semenov, P. Ranitovic, C. L. Cocke, T. Osipov, H. Adaniya, J. C. Thompson, M. H. Prior, A. Belkacem, A. L. Landers, H. Schmidt-Boecking, and R. Doerner, Science **318**, 949 (2007).

[27] T. Jahnke, H. Sann, T. Havermeier, K. Kreidi, C. Stuck, M. Meckel, M. Schoeffler, N. Neumann, R. Wallauer, S. Voss, A. Czasch, O. Jagutzki, A. Malakzadeh, F. Afaneh, T. Weber, H. Schmidt-Boecking, and R. Doerner, Nat Phys **6**, 74 (2010).

[28] A. Knapp, A. Kheifets, I. Bray, T. Weber, A. L. Landers, S. Schossler, T. Jahnke, J. Nickles, S. Kammer, O. Jagutzki, L. Schmidt, T. Osipov, J. Rosch, M. H. Prior, H. Schmidt-Bocking, C. L. Cocke, and R. Dorner, Phys Rev Lett **89**, (2002).

[29] X. Zhou, P. Ranitovic, C. W. Hogle, J. H. D. Eland, H. C. Kapteyn, and M. M. Murnane, Nature Physics **8**, 232 (2012).

[30] S. Hellmann, T. Rohwer, M. Kallaene, K. Hanff, C. Sohrt, A. Stange, A. Carr, M. M. Murnane, H. C. Kapteyn, L. Kipp, M. Bauer, and K. Rossnagel, Nat Comms **3**, (2012).

[31] S. Backus, C. G. Durfee III, M. M. Murnane, and H. C. Kapteyn, Review of Scientific Instruments **69**, 1207 (1998).

[32] R. Dörner, V. Mergela, O. Jagutzkia, L. Spielbergera, J. Ullrichb, R. Moshammerb, and H. Schmidt-Böckinga, Physics Reports **330**, 95 (2000).

[33] X. M. Tong and N. Toshima, Phys Rev A **81**, 063403 (2010).

[34] M. Swoboda, T. Fordell, K. Klunder, J. M. Dahlstrom, M. Miranda, C. Buth, K. J. Schafer, J. Mauritsson, A. L'Huillier, and M. Gisselbrecht, Phys Rev Lett **104**, 103003 (2010).

[35] P. Ranitovic, X. M. Tong, C. W. Hogle, X. Zhou, Y. Liu, N. Toshima, M. M. Murnane, and H. C. Kapteyn, Phys Rev Lett **106**, 053002 (2011).

[36] X. Tong and C. Lin, J Phys B-at Mol Opt **38**, 2593 (2005).

[37] X. M. Tong, P. Ranitovic, C. L. Cocke, and N. Toshima, Phys Rev A **81**, 021404 (2010).

[38] X. M. Tong, P. Ranitovic, C. W. Hogle, M. M. Murnane, H. C. Kapteyn, and N. Toshima, Phys Rev A **84**, 013405 (2011).

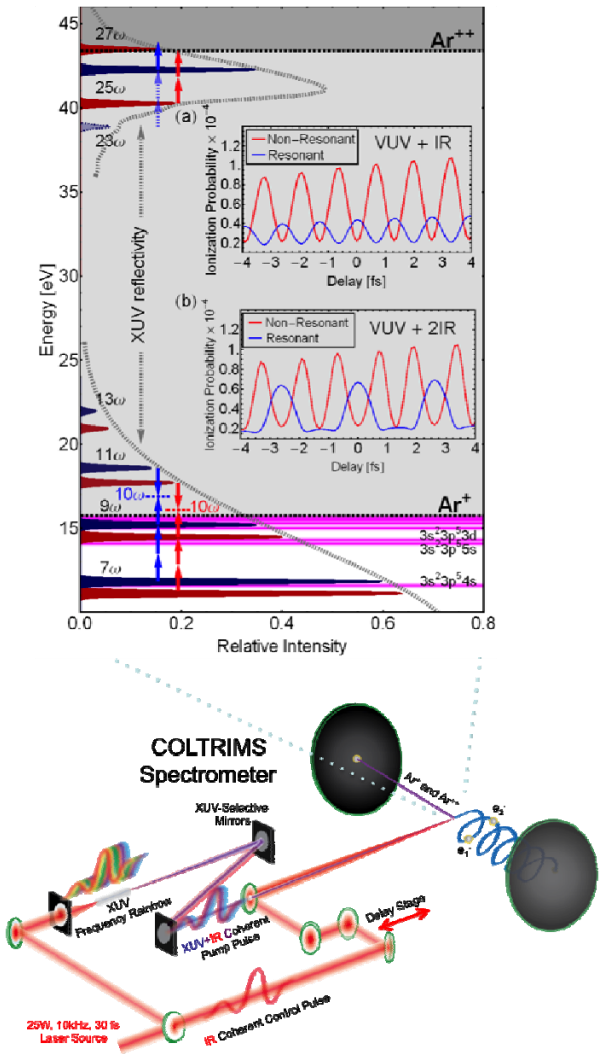

Figure 1: Experimental setup (left) and energy level diagram (right) showing both the relative amplitudes of the harmonics used in the calculation, as well as the relevant energy levels near the single and double ionization threshold of Ar. Multilayer mirrors spectrally select VUV (7ω, 9ω, and 11ω) and XUV (25ω, 27ω) harmonics. Changes in gas pressure, due to the increase of the plasma term in the waveguide, can continuously blue-shift the central energy of the harmonic comb, making it more or less resonant with the Ar^* Rydberg states, as indicated in red and blue respectively. Pressure tuning can also select whether one (25ω) or two (25ω and 27ω) harmonics excite/ionize Ar^+/Ar^{++} around the double ionization threshold. Inset (a) shows the calculated Ar^+ yield for resonant and nonresonant excitation using a VUV pump and IR probe. Inset (b) shows a change in the periodicity of the Ar^+ yield when an additional weak IR pump pulse is added and locked in phase with the VUV pump pulse. The reflectance of the multilayer mirrors is shown in dashed gray.

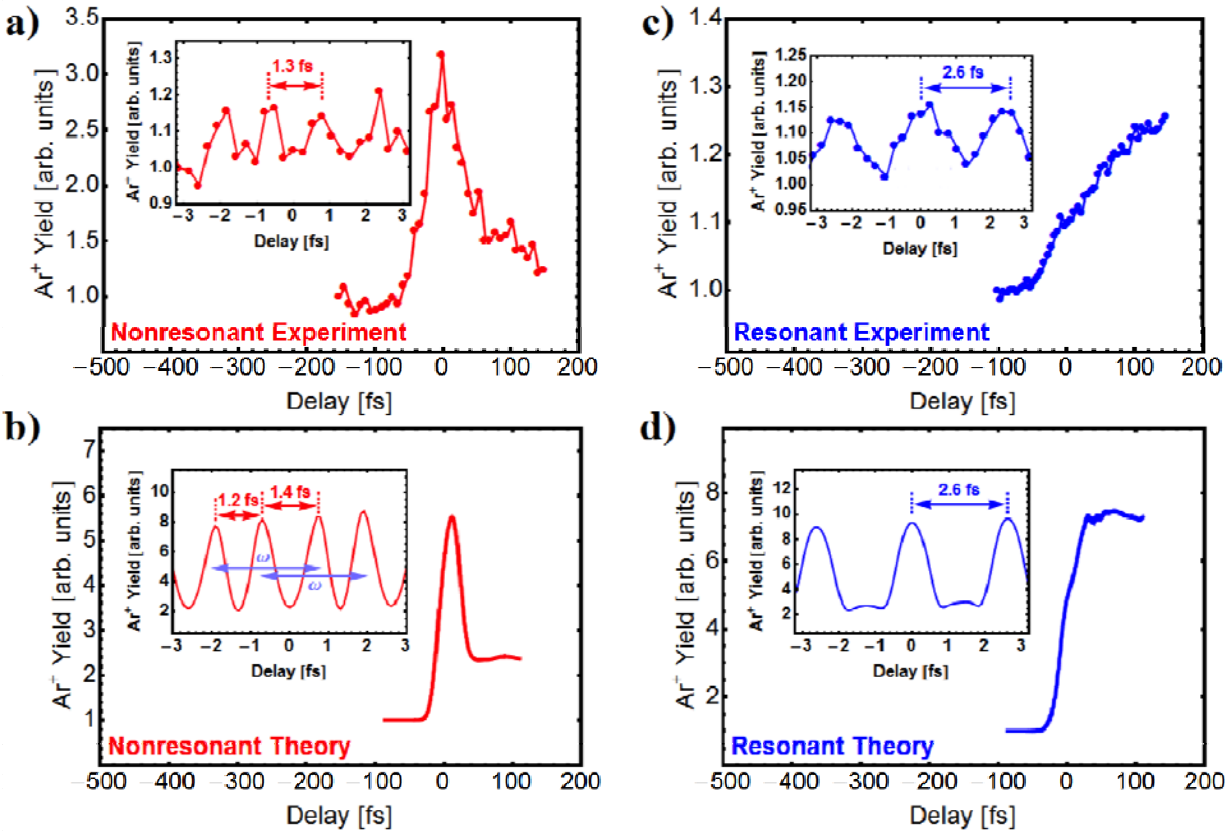

Figure 2: Experimental and theoretical Ar^+ yields as the time delay between the VUV/IR pump and IR probe is varied. The insets enlarge the region near time-zero, on attosecond time scales. **(a)** Ar^+ yield when the 7^{th} and 9^{th} harmonics are mostly not resonant with Ar^* states, while **(b)** shows the corresponding theoretical calculation. **(c)** Ar^+ yield when the 7^{th} and 9^{th} harmonics are resonant with Ar^*, and **(d)** Corresponding simulation. Both **(a,b)** show an Ar^+ yield enhancement only when the pump and probe pulses are overlapped, and exhibit half-cycle oscillations. In contrast, **(c,d)** show step-like enhancement of the Ar^+ yield, as well as full-cycle oscillations of the yield.

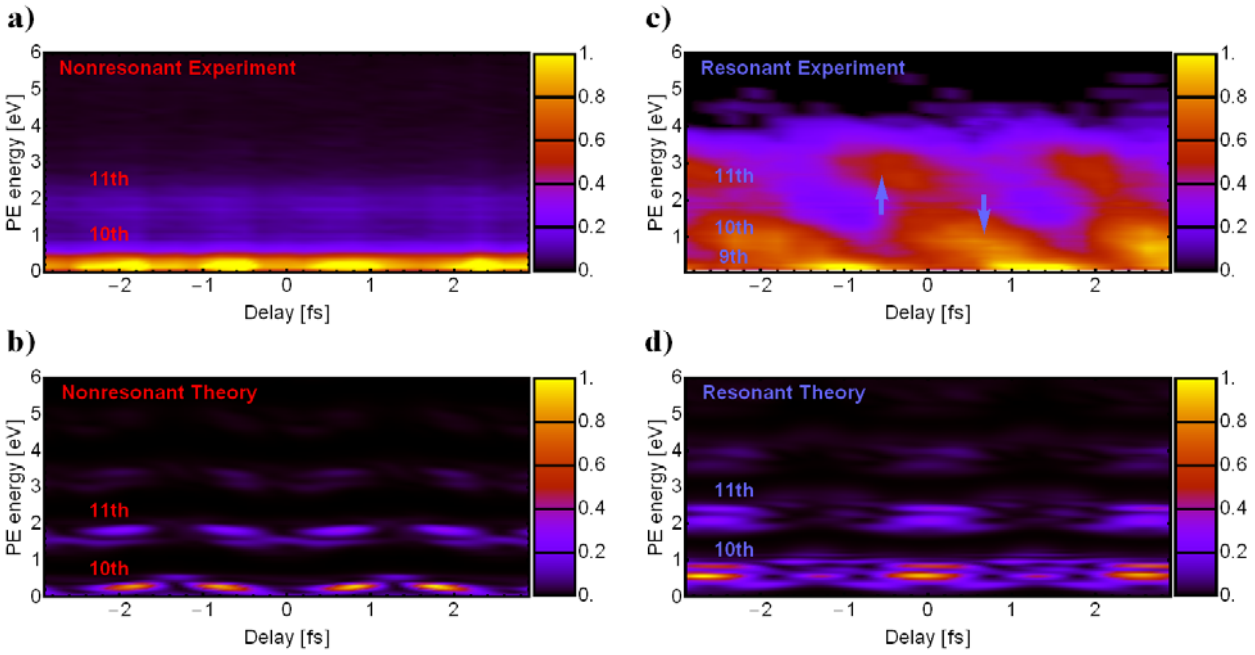

Figure 3: Photoelectron energies taken in coincidence with the Ar^+ yield for nonresonant excitation are shown in **(a)** experiment and in **(b)** simulation. Both exhibit half-cycle oscillations. **(c, d)** Experimental and theoretical photoelectron energies for the case of resonant excitation, with the HHG blue shifted to higher energy, where both exhibit full cycle oscillations. For both nonresonant and resonant excitation, the 10ω band appears only when the probe IR field is present and coincides with the Ar^+ yield enhancement shown in Fig. 2.

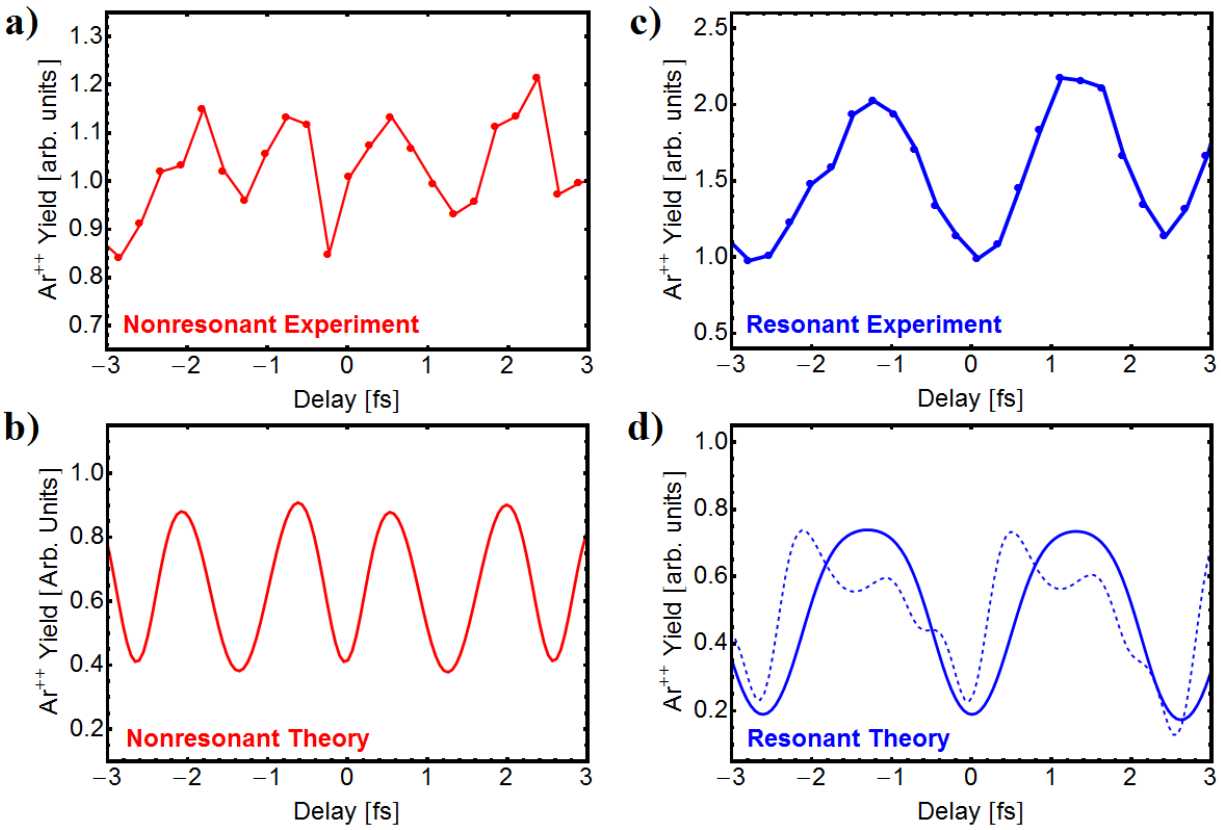

Figure 4: Ar^{++} yield modulation under non-resonant excitation: **(a)** experiment, **(b)** theory. **(c, d)** Ar^{++} yields in the case of resonant excitation, when the VUV harmonics are resonant with Ar^{*} Rydberg states. For non-resonant excitation, both 25ω and 27ω are reflected from the XUV mirror, while in the blueshifted (resonant) case, only 25ω is strongly reflected, as shown in Fig. 1. The dashed line in **(d)** includes a small amplitude 23ω, that modulates Ar^{++} due to two-pathway quantum interferences via resonant excitation.